J Solid State Electrochem (2014) 18:1223–1229
DOI 10.1007/s10008-013-2180-6

ORIGINAL PAPER

Impact of the Pt catalyst on the oxygen electroreduction reaction kinetics on various carbon supports

S. Sepp · E. Härk · P. Valk · K. Vaarmets · J. Nerut · R. Jäger · E. Lust

Received: 30 May 2013 / Revised: 5 July 2013 / Accepted: 7 July 2013 / Published online: 23 July 2013

Abstract Micro- and mesoporous carbide-derived carbons synthesized from molybdenum and tungsten carbides were used as porous supports for a platinum catalyst. Synthesized materials were compared with commercial Vulcan XC72R conducting furnace black. The scanning electron microscopy, X-ray diffraction, Raman spectroscopy, high-resolution transmission electron microscopy, and low-temperature N_2 adsorption methods were applied to characterize the structure of catalysts prepared. The kinetics of oxygen electroreduction in 0.5 M H_2SO_4 solution was studied using cyclic voltammetry and rotating disk electrode methods. The synthesized carbide-derived carbons exhibited high specific surface area and narrow pore size distribution. The platinum catalyst was deposited onto the surface of a carbon support in the form of nanoparticles or agglomerates of nanoparticles. Comparison of carbide-derived carbons and Vulcan XC72R as a support showed that the catalysts prepared using carbide-derived carbons are more active towards oxygen electroreduction. It was shown that the structure of the carbon support has a great influence on the activity of the catalyst towards oxygen electroreduction.

Keywords PEMFC cathode · Oxygen reduction reaction · Pt catalyst · Carbide-derived carbon support

S. Sepp · E. Härk · P. Valk · K. Vaarmets · J. Nerut · R. Jäger · E. Lust (✉)
Institute of Chemistry, University of Tartu, 14a Ravila Str, 50411 Tartu, Estonia
e-mail: enn.lust@ut.ee

Introduction

The slow oxygen electroreduction reaction (ORR) on Pt catalysts is the limiting process for the energy conversion efficiency of the proton exchange membrane fuel cell. Alternative materials are therefore being sought for fuel cell applications. Improved cathode catalysts could have a huge positive impact on fuel cell efficiency [1–4]. Different carbon supports have been tested during long-term catalyst optimization studies [5–11]. In this work, various carbide-derived carbons (CDCs) were compared with the commercial carbon Vulcan XC72R (given below as Vulcan, Cabot Corporation, Boston, MA) [8, 11–14]. CDCs are unique materials in which pore size, shape, uniformity, and other parameters can be controlled in a very exact manner [8, 10–17]. CDCs have been synthesized within the temperature range 200 to 1,200 °C as powders [12], thin-layer coatings, and membrane parts with near-final shapes, with or without mesopores. They may be used as molecular sieves, materials for gas storage devices, catalysts, absorbents/adsorbents, battery and supercapacitor electrodes, and water/air filters and for medical applications [10]. CDCs with incorporated platinum nanoparticles are highly active towards oxygen electroreduction [15–17]. It has been suggested that CDCs are viable fuel cell catalyst supports that are capable of realizing the full activity of Pt nanoparticles with superior corrosion stability [15–18].

The main aim of this work was to study the impact of a Pt catalyst deposited onto the carbon support prepared from WC [12] and Mo_2C [13] and onto Vulcan XC72R powder for comparison. Oxygen electroreduction kinetics was analyzed in 0.5 M H_2SO_4 aqueous solution. The CDCs studied have similar specific surface area, but they differ from one another

in their structural properties, such as pore size distribution and the ratio of micro- and mesopore volumes [10–17]. Therefore, the influence of mesoporosity, pore shapes, and volumes as well as graphitization level on the ORR kinetics has been analyzed.

Experimental details

Preparation of catalyst support

Catalyst supports were synthesized from the metal carbides using the chlorination method at different fixed temperatures from 800 to 1,100 °C [10–13]:

$$x\mathrm{MC}(s) + y/2\,\mathrm{Cl}_2(g) \rightarrow \mathrm{M}_x\mathrm{Cl}_y(g) + \mathrm{C}(s), \quad (1)$$

where M is molybdenum or tungsten cation. The starting materials were Cl_2 (99.99 %, Eesti AGA AS, The Linde Group, Germany), tungsten carbide (α–WC, 99 % purity, particle size <10 μm, Aldrich), and molybdenum carbide (Mo_2C, Sigma-Aldrich, −325 mesh powder). The chlorination temperature for Mo_2C was 800 °C and for WC 1,100 °C, selected on the basis of our earlier data for electrical double-layer capacitors [11–14]. After chlorination, the reactor was flushed with a slow stream of argon to remove the excess of chlorine and residues of gaseous by-products from the nanoporous carbon formed. Additional cleaning treatment with H_2/He (1:4) or H_2/Ar (1:4) mixture was performed at 800 °C during 2 h to remove the residual chlorine, chlorides, and oxygen-containing functional groups from the surface of porous CDC powder. The corresponding carbide-derived carbons are noted below as C(Mo_2C) and C(WC) [8, 11–13].

Preparation of Pt catalyst

The Pt catalyst was deposited onto C(Mo_2C) and C(WC) by the so-called sodium borohydride reduction method [5, 9, 16, 17, 19, 20]. The required quantity of $H_2PtCl_6 \times 6H_2O$ (99.9 %, Alfa Aesar) was dissolved in Milli-Q^+ water, and the mixture was diluted to prepare a solution with a total Pt cation concentration of ~2 mM. The solution was thereafter stirred at ambient temperature for 1 h. The pH of the solution was adjusted to ~8 with dropwise addition of 20 wt % NaOH (99.99 %, Sigma-Aldrich) solution. The required amount of carbon substrate (C(Mo_2C) [13, 14], C(WC) [10, 11], or Vulcan XC72R) was suspended in Milli-Q^+ water and stirred to form a homogeneous carbon slurry, which was added into an aqueous solution of H_2PtCl_6. Thereafter, the $NaBH_4$ (≥98.0 %, Aldrich) solution was prepared by dissolving $NaBH_4$ in Milli-Q^+ water, and the solution was added carefully into the previously prepared suspension. The received reaction mixture was stirred for 2 h and left to settle overnight. The catalyst was filtered, rinsed thoroughly by Milli-Q^+ water, and dried in a vacuum oven at 80 °C. The amount of Pt in the catalyst was ~60 wt %. The prepared catalysts will be denoted as Pt-C(Mo_2C), Pt-C(WC), and Pt-C(Vulcan).

Preparation of catalyst ink and electrodes

Glassy carbon disk electrodes (GCDEs), pressed into a Teflon holder, were used as the support for each catalyst layer (diameter 5 mm). The GCDE was polished with 0.05 μm alumina slurry (Buehler) to a mirror finish. After polishing, the GCDE was washed with Milli-Q^+ water and sonicated in Milli-Q^+ water for a few minutes. Catalyst ink was prepared by suspending the catalyst in Milli-Q^+ water by agitation in an ultrasonic bath for 30 min to wet and disperse the catalyst thoroughly and homogeneously. Nafion® dispersion solution (Aldrich) was then added (5 wt %) into the catalysts mixture (to give a dry ink with fixed 5 wt % of Nafion® ionomer) and sonicated for 2 h at room temperature to obtain uniformly dispersed ink. The catalyst ink was deposited onto the GCDE surface and dried at room temperature.

The flat cross-sectional surface (geometric) area of the electrode was 0.196 cm^2, and the thickness of the catalyst layer was nearly 30 μm. The loading of the Pt-C catalyst on GCDE was approximately 0.5 mg cm^{-2} (thus, ~0.3 mg Pt per 1 cm^2 geometric surface area). In order to achieve a good wetting of the catalyst layers, the electrode was impregnated in Milli-Q^+ water before the assembling of the electrochemical cell.

Cyclic voltammetry and rotating disk electrode experiments

The electrochemical measurements were carried out in a three-electrode electrochemical cell [1, 21, 22] using a rotating disk electrode (RDE) system (Pine Instrumental Company). A potentiostat/galvanostat Autolab PGSTAT 302 (Eco Chemie B.V.) was used for cyclic voltammetry (CV) and ac impedance [19] measurements. The electrochemical conditions were controlled with General Purpose Electrochemical System and Frequency Response Analyser software. The counter electrode was a large Pt wire mesh, separated from the main solution by a fritted glass membrane. The working electrode potential was measured against the $Hg|Hg_2SO_4|$ saturated K_2SO_4 reference electrode, connected to the cell through a long Luggin capillary. Data were converted to the standard hydrogen electrode (SHE) scale, and hereafter, all potentials are given vs. SHE.

The electrodes were submerged in 0.5 M H_2SO_4 (Fluka, TraceSelect® Ultra) solution under a standby potential of 1.07 V (vs. SHE), where faradaic current densities were minimal. In prior measurements, the electrode potential was cycled within a potential region from 0.05 to 1.07 V (vs. SHE) in 0.5 M H_2SO_4 aqueous solution saturated with Ar (99.9999 %, Eesti AGA

AS, The Linde Group, Germany) for at least 1 h to achieve a stable surface state. Thereafter, CVs at different potential scan rates, v (so-called background current densities), were collected. After CV measurements, the RDE voltammetry curves (at rotation velocities from 0 to 3,000 rpm) were measured at potential scan rate v=10 mV s^{-1}.

Next, the solution was saturated by high-purity molecular O_2 (99.999 %, Eesti AGA AS, The Linde Group, Germany) for 30 min, and CVs at different v from 2 to 50 mV s^{-1} were obtained. Before the RDE measurements at different rotation velocities and for equilibration of electrode properties, RDE was cycled at least ten times within the potential range from 0.05 to 1.07 V (vs. SHE) at a constant rotation velocity of 800 rpm. Thereafter, RDE measurements were conducted at different RDE rotation velocities to study the ORR kinetics [15–17].

The electrochemical impedance spectroscopy (EIS) data were obtained at ac frequencies from 10 to 1×10^{-5} kHz at 0.65 V (vs. SHE) with potential modulation of ±5 mV. The electrolyte resistance, i.e., the high-frequency series resistance $R_{ex}=Z'$, was calculated from EIS data at $f\rightarrow\infty$, and it was used to correct the measured electrode potentials against ohmic potential drop in the solution phase between the electrode and the tip of the Luggin capillary.

All measurements were carried out at temperature 22±1 °C, and at least four different electrodes, prepared using identical conditions, were tested [15–17].

Results and discussion

Physical characterization

All materials were characterized by scanning electron microscopy. The calculated particle size of a catalyst support varies from 1 to 7 μm. Modification of catalyst support with nanoparticles of platinum did not change noticeably the particle size and structure of the powder [15, 16].

The first-order Raman spectra of perfectly ordered monocrystalline carbon (i.e., graphite) show one peak at ~1,587 cm^{-1}, whereas disordered amorphous carbon generally shows two peaks [8, 10, 13, 14]: a so-called graphite (G) peak at ~1,587 cm^{-1} and disorder-induced (D) peak at ~1,348 cm^{-1} (Fig. 1). The G peak corresponds to sp_2 inplane vibrations with E_{2g} symmetry. The Raman spectrum also shows the second-order peak of the D band (2D) at ~2,700 cm^{-1}. The increase in the 2D peak is related to the crystallographic ordering of the graphitic structure. The carbon synthesized from molybdenum carbide at 800 °C is more amorphous, as can be seen from the comparison of the relative intensities of the 2D peak (Fig. 1). This result is confirmed also by the comparison of the intensities of D and G peaks, i.e., the intensity of D peak for C(WC) is considerably higher compared with that of the G peak. The

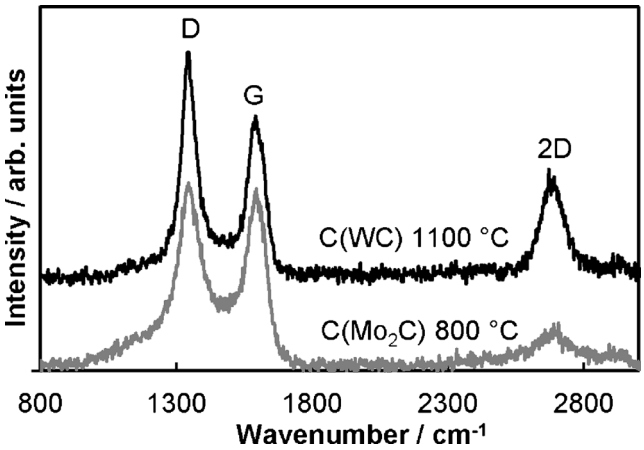

Fig. 1 Raman spectra for C(WC) and C(Mo_2C) powders, normalized by the G peak intensities

Tuinstra–Koening method has been used to estimate the inplane correlation length L_a [12, 23, 24]:

$$\frac{I_D}{I_G}=\frac{C(\lambda)}{I_G}, \quad (2)$$

where I_D/I_G is the ratio of the intensities of D and G peaks, respectively, and $C(\lambda)$ is a wavelength-dependent parameter (at fixed λ=514 nm, it is equal to 4.36). The average size of C(WC) crystallites obtained (L_a=4.4 nm) is slightly higher compared with that for C(Mo_2C) (L_a=3.4 nm). The apparent crystallite sizes along c and a directions of the graphite structure, calculated from the XRD data (not shown for shortness) using Debay–Scherrer equations [9, 10], agree with the analysis of Raman spectra for CDCs under study [12, 13].

Pt-C(Mo_2C) was studied using a high-resolution transmission electron microscope (HRTEM, Tecnai 12 operating at the 120-V accelerating voltage). The data in Fig. 2a show that C(Mo_2C) is mainly amorphous, presenting only little evidence of interlayer correlation. On the other hand, the HRTEM micrograph of a graphene-like C(WC) particle (Fig. 2b) reveals the existence of somewhat ordered graphitic particles in the sample. Deposited platinum (Fig. 2c) has formed mainly small and clearly separated nanoparticles (d<5 nm); however, some Pt agglomerates in some areas of C(Mo_2C) have been observed as well.

The porous structure of a carbon support was characterized by using the nitrogen sorption method. The low-temperature N_2 adsorption/desorption experiments were performed at the boiling temperature of liquid nitrogen (−195.8 °C) using the ASAP 2020 system (Micromeritics) [12, 13]. The corresponding isotherms for C(Mo_2C) and C(WC) show that the adsorption data can be approximated by the isotherm known as type IV isotherm with H4 type hysteresis (IUPAC classification), caused by the capillary condensation of nitrogen in the mesopores. The specific surface area (S_{BET}), pore width, micropore volume (V_{micro}),

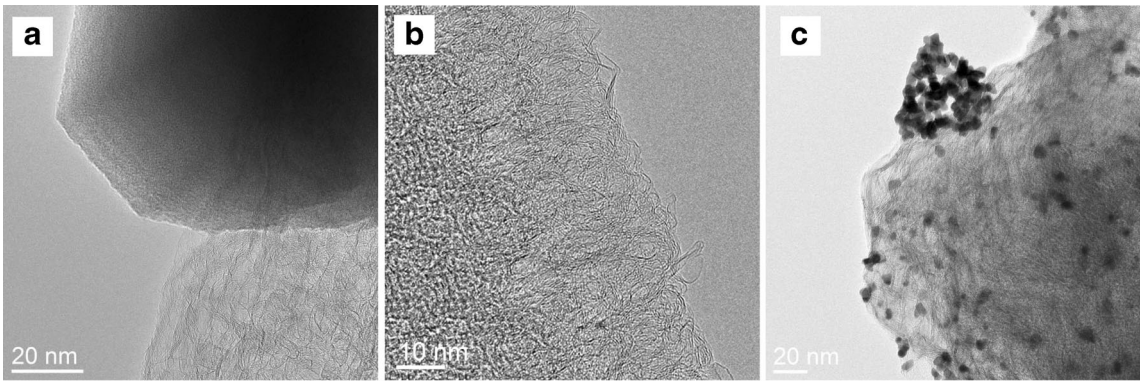

Fig. 2 High-resolution transmission electron microscopy data for **a** pure carbon support C(Mo_2C), **b** pure carbon support C(WC), and **c** Pt nanocluster catalyst, deposited onto carbon support C(Mo_2C)

total pore volume (V_{tot}), and other parameters (not shown for shortness) for porous carbon materials were calculated according to the Brunauer–Emmett–Teller (BET) and nonlocal density functional theories (NLDFT), as well as applying the t-plot method [12, 13, 25].

According to the data in Table 1, both synthesized carbon supports have comparatively high specific surface area and are mainly microporous, but some mesoporosity has been observed for C(Mo_2C). BET surface area for Vulcan XC72R is almost seven times smaller than the surface area for studied CDCs, but Vulcan XC72R is mostly a mesoporous material. Dependencies of differential pore size distribution on pore width (Fig. 3) reveal complicated shape with two or three clearly expressed maxima. C(Mo_2C) has wider pores compared with C(WC). After the modification of carbon support with Pt nanoparticles, the surface area was reduced noticeably [15, 16].

Electrochemical characterization

CV and RDE data (corrected for Ar-saturated system current densities, i.e., for so-called background current densities) show that high cathodic O_2 electroreduction current densities have been achieved for the Pt nanocluster-modified electrodes deposited onto the GCDE support (Fig. 4). For Pt-C(Mo_2C) electrode, the overvoltage of ORR is about 0.5 V lower than that for pure catalyst support C(Mo_2C). The formation of clear diffusion-limited current plateaus takes place for the ORR on Pt-C(Mo_2C), Pt-C(WC), and Pt-C(Vulcan). In the case of nonactivated C(Mo_2C), C(WC), or C(Vulcan), the ORR current is only just approaching the plateau region, and the absolute values of the current for C(Mo_2C) are about two times lower than the corresponding values for Pt-C(Mo_2C).

The kinetic current densities, j_k, were calculated from the linear Koutecky–Levich plots (Fig. 5) and analyzed using the Koutecky–Levich equation [1, 21]

$$\frac{1}{j} = \frac{1}{j_k} + \frac{1}{j_D} = -\frac{1}{nFk_{het}c^b_{O_2}} - \frac{1}{0.62nFD_{O_2}{}^{2/3}c^b_{O_2}\upsilon^{-1/6}\omega^{1/2}}, \quad (3)$$

where j is the current density corrected for current density measured at reference (background) conditions, j_D is the diffusion step-limited current density, n is the number of electrons transferred per oxygen molecule electroreduction, F is the Faraday constant, $c^b_{O_2}$ is the concentration of oxygen in the bulk solution, k_{het} is the electrochemical rate constant for ORR, D_{O_2} is the diffusion coefficient for oxygen, υ is the kinematic viscosity of the solution, and ω is the angular frequency (radian per second) of the electrode. The number of electrons transferred per oxygen molecule electroreduction for unmodified carbon materials was determined from Eq. (3). For Pt-modified materials, the number of electrons transferred was calculated within the diffusion-limited potential region. Linear Koutecky–Levich plots for Pt-C(Mo_2C) and Pt-C(WC) are presented in Fig. 5 in the potential region from 0.79 to 0.59 V (vs. SHE). Panels a and b of Fig. 6 demonstrate the

Table 1 Results of sorption measurements for C(Mo_2C) and C(WC)

S_{BET} BET surface area, V_{micro} micropore volume, V_{tot} total pore volume

Material	S_{BET} (m^2 g^{-1})	V_{micro} (cm^3 g^{-1})	V_{tot} (cm^3 g^{-1})
C(Mo_2C) 800 °C	1,675	1.179	1.399
C(WC) 1,100 °C	1,580	0.83	0.89
Vulcan XC72R	240	0.07	0.83

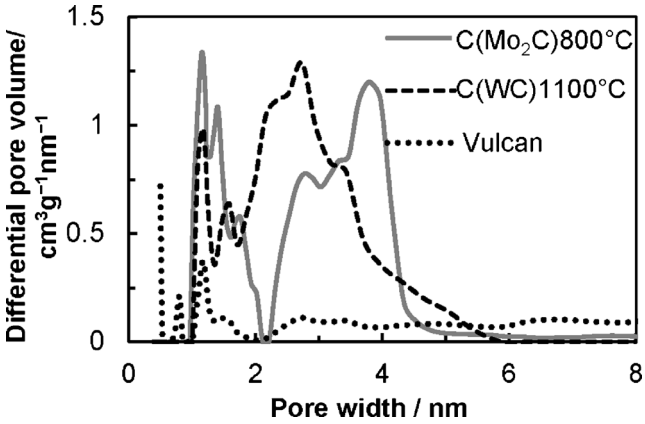

Fig. 3 Differential pore size distribution vs. pore width plots for C(WC), C(Mo_2C), and Vulcan XC72R, obtained using NLDFT method

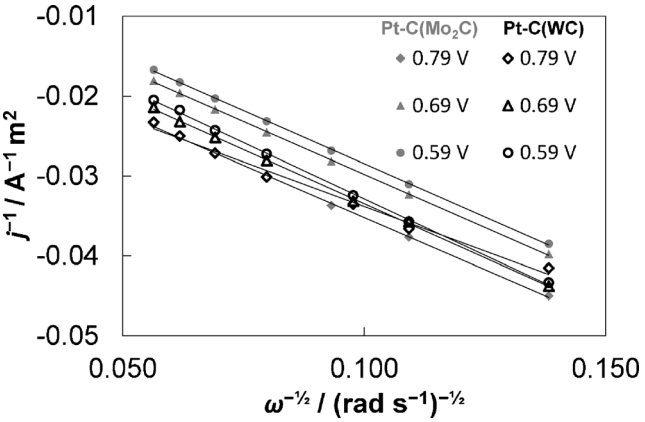

Fig. 5 Koutecky–Levich plots for Pt-C(Mo_2C) (*filled markers*) and Pt-C(WC) (*empty markers*) in 0.5 M H_2SO_4 solution. Potentials vs. SHE are given in the figure

potential dependence of the logarithm of the ORR kinetic current density and number of electrons, respectively, for all materials studied. The electroreduction currents of O_2 for the less-ordered C(Mo_2C) electrode are higher in the range of studied potentials compared with those for C(WC) (Fig. 6a). Vulcan XC72R shows approximately one order of magnitude lower kinetic currents (at 0.15 V) than those established for CDCs. More amorphous C(Mo_2C) has more crystallographic defects and edge planes in the structure [11–16], which are catalytically active centers for the ORR. It has been shown that the current-vs.-voltage curve for oxygen reduction on the edge plane pyrolytic graphite is shifted by around 0.45 V towards higher positive potentials than that for the C(0001) basal plane [26]. It should be noted that if the platinum nanoclusters are deposited onto the carbon support, the difference in activities of Pt-C(Mo_2C) and Pt-C(WC) becomes more evident as the half-wave potential shifts in a more negative direction, indicating that Pt-C(Mo_2C) has a larger number of catalytic sites. However, it is interesting that the overvoltage for the ORR on Pt-C(Mo_2C) and on Pt-C(WC) is quite similar. Another reason for the greater activity of C(Mo_2C) and Pt-C(Mo_2C) might be the structure of carbon support, i.e., the more mesoporous C(Mo_2C) structure facilitates more rapid transport of oxygen molecules within the micromesoporous material layer of the electrode.

The number of electrons transferred per one oxygen molecule (Fig. 6b) has been calculated from the slope of Koutecky–Levich Eq. (3), using the parameters: $c^{b}_{O_2} = 1.3 \times 10^{-6}$mol cm^{-3}, $D_{O_2} = 1.8 \times 10^{-5}$cm^2 s^{-1}, and $\upsilon = 0.01$ cm^2 s^{-1} [6, 21]. Characteristically for a nonactivated carbon support, the number of electrons transferred for the ORR on C(Mo_2C) and C(WC) is approximately two [26]. Thus, the main reaction product of ORR on the nonactivated carbons is hydrogen peroxide:

$$O_2 + 2H^+ + 2e^- = H_2O_2 \quad (4)$$

This agrees well with the data in Fig. 4, where the height of the current plateau for the ORR on C(Mo_2C) is about two

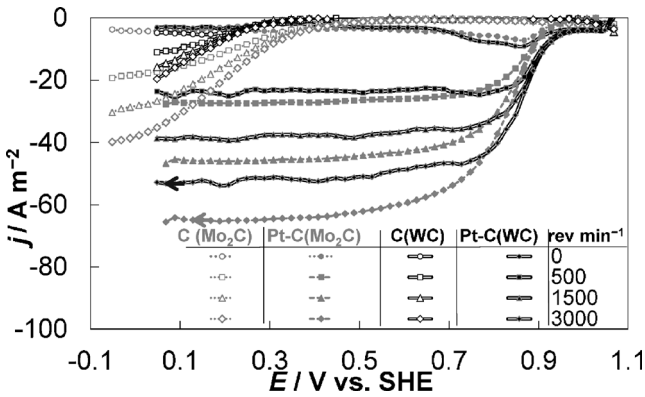

Fig. 4 The oxygen reduction current vs. electrode potential for studied CDCs (*empty markers*) and for Pt-CDCs (*filled markers*) in 0.5 M H_2SO_4 solution at different electrode rotation rates (in revolution per minute) given in the figure. Currents are corrected for current densities in 0.5 M H_2SO_4 solution, saturated with Ar

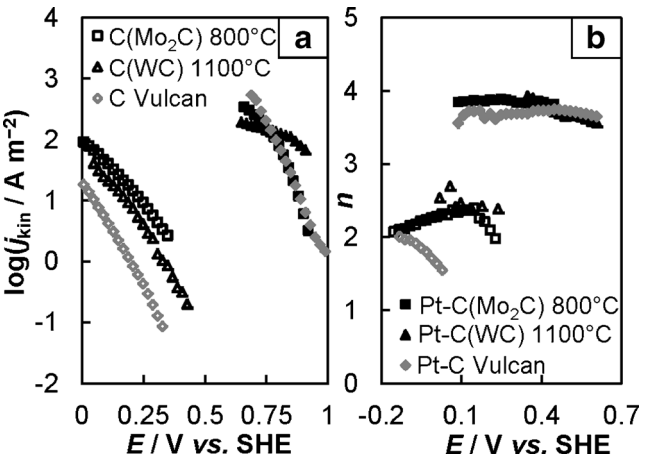

Fig. 6 **a** Dependence of the logarithm of kinetic current density and **b** number of electrons transferred per one oxygen molecule electroreduction vs. electrode potential for nonactivated carbon supports (*empty markers*) and for Pt-C catalysts (*filled markers*) in 0.5 M H_2SO_4 solution

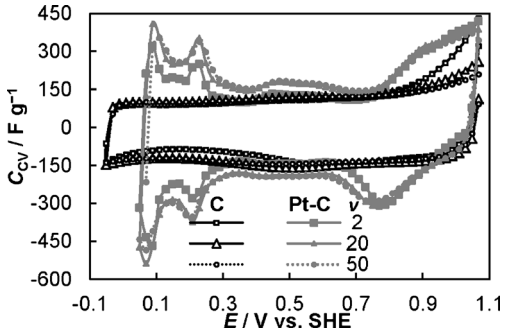

Fig. 7 Capacitance vs. electrode potential curves for C(Mo_2C) (*empty markers*) and Pt-C(Mo_2C) electrodes (*filled markers*) in 0.5 M H_2SO_4 solution at different potential scan rates ν (in millivolt per second), given in the figure. Currents are uncorrected for current densities in 0.5 M H_2SO_4 solution saturated with ArA

times lower than that on Pt-C(Mo_2C). A similar result was obtained on pyrolytic graphite in 0.1 M H_2SO_4 solution [26].

The ORR on Pt-C(Mo_2C) or on Pt-C(WC) is nearly ideally a four-electron process, i.e., the main product of ORR is water.

$$O_2 + 4H^+ + 4e^- = 2H_2O \tag{5}$$

Data in Fig. 5b show that for ORR on Pt-C(WC), the number of transferred electrons starts to decrease as the potential becomes more positive than 0.16 V vs. SHE.

The gravimetric capacitance C_{CV} values were calculated from the CV curves (Fig. 7). As the specific surface area for carbon support is very high, the behavior of the system is highly capacitative. Analysis of CV data shows that high-capacitance C_{CV} values (150 F g^{-1}) have been established for both CDC and Pt-CDC electrodes. Cycling the potential from negative towards positive potentials, the carbon support starts to oxidize at E more positive than 0.90 V vs. SHE. For Pt nanocluster-activated CDC, distinct regions of cathodic hydrogen evolution and adsorption–desorption of hydrogen (cathodic scan, E<0.30 vs. SHE) and surface oxide formation (anodic scan, E>0.85 V vs. SHE) can be observed. Systematic analysis of data shows that the hydrogen evolution overpotential is highest for C(Vulcan) and lowest for C(Mo_2C), explained by a more optimal structure of microporosity/mesoporosity, density of defects, etc., of the carbon electrode. The same order of activity of electrodes is valid for Pt nanocluster-modified electrodes, deposited onto glassy carbon support. Hydrogen evolution and ORR cause intensive pseudocapacitative behavior, i.e., the value of specific capacitance increases up to 500 F g^{-1}. Thus, Pt-CDC catalysts are interesting electrode materials for polymer electrolyte fuel cells and hybrid supercapacitor systems. At more negative potentials than 0.0 vs. SHE, intense evolution of hydrogen starts.

To estimate the catalytically active surface area of Pt-CDC and Pt-Vulcan XC72R catalysts, C_{CV} values have been integrated within the potential region of evolution and adsorption–desorption peaks of hydrogen. The utilization of a Pt-CDC catalyst can be deduced from the comparison of the electrochemically active area with the number of exposed Pt surface atoms calculated from the Pt loading and the Pt nanocluster dispersion [3]. The number of Pt surface atoms is estimated from the coulombic charge values of hydrogen adsorption or desorption Q_H (in C g−1) within the potential region 0.05 V<E<0.35 V vs. SHE. One adsorbed H_{ad} per Pt surface atom has been assumed, and therefore, the hydrogen adsorption charge can be determined via equation

$$Q_H = Q_{total} - Q_{DL}, \tag{6}$$

where Q_{total} is the total charge transferred within the hydrogen adsorption or desorption potential region, and Q_{DL} is the charge calculated from the capacitance vs. E-data for the high-surface-area carbon support. As the capacitance values for Pt-CDC and CDC are very close in the so-called double-layer region (0.35<E<0.65), Q_{DL} was calculated from C_{CV}, E-curve measured for the pure carbon support. The corresponding calculated charges for hydrogen adsorption or desorption and average Q_H values are given in Table 2. The Pt nanocluster dispersion ratio was calculated using the equation

$$\text{Dispersion} = \frac{Q_H \cdot A_{Pt}}{F}, \tag{7}$$

where A_{Pt} is the atomic mass of Pt. It was found that the dispersion of platinum on C(Mo_2C) is about 6 % higher than that on C(WC), explaining why the ORR proceeds faster on Pt-C(Mo_2C) than on Pt-C(WC). Assuming that the Pt particles have normal metallic densities and they form ideal spheres, the average particle diameter d has been calculated (Table 2).

Table 2 The charges for hydrogen adsorption and desorption, the dispersion, and the size of Pt particles on modified materials

Material	Q_H (C g^{-1})			Dispersion (%)	Particle diameter (nm)
	Adsorption	Desorption	Average		
Pt-C(Mo_2C) 800 °C	201	176	189	38	3.6
Pt-C(WC) 1,100 °C	171	150	161	32	4.3
Pt-C Vulcan	87	84	85	17	7.7

Additionally, it was supposed that the whole Pt surface consists of the closely packed Pt(111) plane, on which the effective area of one Pt atom is 6.55 $Å^2$ [27].

Conclusion

Micromesoporous CDCs have been synthesized from Mo_2C and WC powders by chlorination at temperatures 800 and 1,100 °C, respectively. Comparison of the data for the materials prepared and commercial carbon Vulcan XC72R (C(Vulcan)) show that carbon derived from WC is more graphitized and more microporous compared with that from Mo_2C, but C(Vulcan) is mainly mesoporous. Different graphitization levels probably cause higher ORR overpotentials on the porous carbon electrode derived from WC. The hydrogen evolution overpotential is highest for C(Vulcan). Thus, the synthesized carbide-derived carbons are more active for the ORR and demonstrate higher kinetic current density values than C(Vulcan).

Pt nanocluster-activated Pt-CDCs and Pt-C(Vulcan) have been prepared using so-called sodium borohydride reduction method. Kinetic current density values for the ORR are highest on the Pt-C(Mo_2C) electrode. Due to the more optimal structure of the carbon supports (the number of defects and the ratio of micro- and mesopores), the electrochemical activity of C(Mo_2C) is higher than that of C(WC) and especially that of C(Vulcan). The dispersion analysis of Pt nanoparticles also shows that the rate of the ORR on Pt-C(Mo_2C) is higher, because the catalytically active surface area of Pt-C(Mo_2C) is larger than that of Pt-C(WC) and Pt-C(Vulcan).

Acknowledgments This work was supported by Estonian Target Research Project SF0180002s08, Estonian Energy Technology Program Project SLOKT 10209T, Estonian Centre of Excellence Project 3.2.0101-11-0030, and ESF grant ETF8267. Authors thank J. Eskusson, I. Tallo, H. Kurig, J. Aruväli, and Prof. K. Kirsimägi for performing SEM-EDX, XRD, and BET measurements and analysis of the data. Prof. K. Kontturi from Aalto University is thanked for the help with HRTEM studies.

References

1. Wang B (2005) Recent development of non-platinum catalysts for oxygen reduction reaction. J Power Sources 152:1–15
2. Petrii OA (2008) Pt-Ru electrocatalysts for fuel cells: a representative review. J Solid State Electrochem 12:609–642
3. Schmidt TJ, Gasteiger HA, Stäb GD, Urban PM, Kolb DM, Behm RJ (1998) Characterization of high-surface-area electrocatalysts using a rotating disk electrode configuration. J Electrochem Soc 145:2354–2358
4. Schmidt TJ, Gasteiger HA, Behm RJ (1999) Rotating disk electrode measurements on the CO tolerance of a high-surface area Pt/Vulcan carbon fuel cell catalyst. J Electrochem Soc 146:1296–1304
5. Chai GS, Yoon SB, Yu J-S, Choi J-H, Sung Y-E (2004) Ordered porous carbons with tunable pore sizes as catalyst supports in direct methanol fuel cell. J Phys Chem B 108:7074–7079
6. Gottesfeld S, Raistrick ID, Srinivasan S (1987) Oxygen reduction kinetics on a platinum RDE coated with a recast Nafion film. J Electrochem Soc 134:1455–1462
7. Antolini E (2009) Carbon supports for low-temperature fuel cell catalysts. Appl Catal B Environ 88:1–24
8. Jänes A, Thomberg T, Lust E (2007) Synthesis and characterisation of nanoporous carbide-derived carbon by chlorination of vanadium carbide. Carbon 45:2717–2722
9. Álvarez G, Alcaide F, Miguel O, Calvillo L, Lázaro M, Quintana J, Calderón J, Pastor E (2010) Technical electrodes catalyzed with PtRu on mesoporous ordered carbons for liquid direct methanol fuel cells. J Solid State Electrochem 14:1027–1034
10. Gogotsi Y, Nikitin A, Ye H, Zhou W, Fischer JE, Yi B, Foley HC, Barsoum MW (2003) Nanoporous carbide derived carbon with tunable pore size. Nat Mater 2:591–594
11. Tallo I, Thomberg T, Jänes A, Lust E (2012) Electrochemical behavior of α-tungsten carbide-derived carbon based electric double-layer capacitors. J Electrochem Soc 159(3):A208–A213
12. Tallo I, Thomberg T, Jänes A, Kontturi K, Lust E (2011) Nanostructured carbide-derived carbon synthesized by chlorination of tungsten carbide. Carbon 49:4427–4433
13. Jänes A, Thomberg T, Kurig H, Lust E (2009) Nanoscale fine-tuning of porosity of carbide-derived carbon prepared from molybdenum carbide. Carbon 47:23–29
14. Thomberg T, Jänes A, Lust E (2009) Energy and power performance of vanadium carbide derived carbon electrode materials for supercapacitors. J Electroanal Chem 630:55–62
15. Vaarmets K, Sepp S, Nerut J, Härk E, Tallo I, Lust E (2013) Electrochemical and physical characterization of Pt-Ru alloy catalyst deposited onto microporous-mesoporous carbon support derived from Mo_2C at 600°C. J Solid State Electrochem 17:1729–1741
16. Härk E, Nerut J, Vaarmets K, Tallo I, Kurig H, Eskusson J, Kontturi K, Lust E (2013) Electrochemical impedance characteristics and electroreduction of oxygen at tungsten carbide derived micromesoporous carbon electrodes. J Electroanal Chem 689:176–184
17. Lust E, Härk E, Nerut J, Vaarmets K (2012) Pt and Pt-Ru catalysts for polymer electrolyte fuel cells deposited onto carbide derived carbon supports. Electrochem Acta. doi:10.1016/j.electacta.2012.10.024
18. Borchardt L, Hasché F, Lohe MR, Oschatz M, Schmidt F, Kockrick E, Ziegler C, Lescouet T, Bachmatiuk A, Büchner B, Farrusseng D, Strasser P, Kaskel S (2012) Transition metal loaded silicon carbide-derived carbons with enhanced catalytic properties. Carbon 50:1861–1870
19. Antolini E, Cardellini F (2001) Formation of carbon supported PtRu alloys: an XRD analysis. J Alloys Compd 315:118–122
20. Lakshminarayanan V, Srinivasan R, Chu D, Gilman S (1997) Area determination in fractal surfaces of Pt and Pt-Ru electrodes. Surf Sci 392:44–51
21. Bard AJ, Faulkner LR (2001) Electrochemical methods, 2nd edn. Wiley, New York
22. Macdonald JR (1987) Impedance spectroscopy emphasizing solid materials and systems. Wiley, New York
23. Ferrari AC, Robertson J (2000) Interpretation of Raman spectra of disordered and amorphous carbon. Phys Rev B 61:14095–14107
24. Ferrari AC (2007) Raman spectroscopy of graphene and graphite: disorder, electron–phonon coupling, doping and nonadiabatic effects. Solid State Commun 143:47–57
25. Webb PA, Orr C (1997) Analytical methods in fine particle technology. Micrometrics Instrument Corp, Norcross
26. Gara M, Compton RG (2011) Activity of carbon electrodes towards oxygen reduction in acid: a comparative study. New J Chem 35:2647–2652
27. Bond GC (1975) Small particles of the platinum metals. Platin Met Rev 19:126–134